Food & Function

ROYAL SOCIETY OF CHEMISTRY

PAPER

View Article Online
View Journal | View Issue

Open Access Article. Published on 09 September 2025. Downloaded on 1/11/2026 8:00:54 PM.
This article is licensed under a Creative Commons Attribution-NonCommercial 3.0 Unported Licence.

Check for updates

Cite this: *Food Funct.*, 2025, **16**, 7717

Glycyrrhizin alleviates renal damage in MRL/lpr mice by modulating gut microbiota dysbiosis and regulating the RTK-PKCα axis: insights from reverse network pharmacology

Fugang Huang,†[a] Ke Sun,†[b] Lijia Diao,†[a] Keda Lu,[c] Yongsheng Fan*[d] and Guanqun Xie *[e]

The present investigation elucidates the therapeutic potential of glycyrrhizin, the predominant triterpene saponin isolated from *Glycyrrhiza glabra* (licorice), in the management of systemic lupus erythematosus (SLE), an autoimmune disorder characterized by multisystemic involvement and therapeutic recalcitrance. Comprehensive interrogation of multiple disease-specific databases facilitated the identification of crucial SLE-associated molecular targets and hub genes, with MAPK1, MAPK3, TP53, JUN, and JAK2 demonstrating the highest degree of network centrality. Subsequent molecular docking simulations and binding affinity assessments revealed compounds with exceptional complementarity to these pivotal molecular targets, establishing *Glycyrrhiza glabra* as a pharmacologically promising botanical source and glycyrrhizin as its principal bioactive constituent meriting comprehensive mechanistic investigation. Experimental validation employing the MRL/lpr murine lupus model demonstrated that glycyrrhizin treatment significantly diminished circulating autoantibody titers and markedly ameliorated the characteristic glomerulonephritis and tubular interstitial damage associated with lupus nephritis. Concomitant 16S rDNA gene sequencing-based microbiome profiling revealed that glycyrrhizin administration induced substantial modulation of the intestinal microbial ecosystem, specifically attenuating the abundance of *Ruminococcus* genus, a bacterial taxon previously implicated in the pathogenesis and exacerbation of lupus nephritis. Transcriptomic analysis utilizing Gene Expression Omnibus (GEO) repository datasets confirmed glycyrrhizin's profound regulatory effects on calcium signaling pathways. Mechanistically, glycyrrhizin suppresses renal receptor tyrosine kinase (RTK)-protein kinase C alpha (PKCα) axis activation, thereby interrupting key inflammatory and fibrotic signaling cascades. Collectively, these findings provide compelling evidence that glycyrrhizin confers nephroprotective effects in lupus nephritis through orchestrated dual mechanisms: (1) restoration of gut microbiota homeostasis, and (2) suppression of the renal RTK-PKCα signaling axis, thereby attenuating inflammatory cascades and preserving renal architectural integrity. These mechanistic insights advance our understanding of glycyrrhizin's therapeutic potential and establish a robust scientific foundation for its clinical translation in SLE management strategies.

Received 12th April 2025,
Accepted 28th August 2025

DOI: 10.1039/d5fo01743b

rsc.li/food-function

Introduction

Systemic lupus erythematosus (SLE) stands as a paradigmatic multisystem autoimmune disorder, orchestrating a symphony of pathophysiological disruptions through intricate genetic predisposition, environmental provocations, and pharmacological perturbations. The pathogenetic landscape of SLE unfolds through dysregulated cytokine cascades, wherein type I interferons reign supreme among pro-inflammatory mediators, synergistically amplified by complement system dysregulation.[1] This molecular tempest precipitates ubiquitous immune complex deposition, weaving a tapestry of chronic inflammation that manifests through diverse clinical pheno-

[a]*The First School of Clinical Medicine, Zhejiang Chinese Medical University, Hangzhou 310053, P.R. China. E-mail: xieguanqun2025@163.com*
[b]*The Third School of Clinical Medicine, Zhejiang Chinese Medical University, Hangzhou 310053, P.R. China*
[c]*The Third Affiliated Hospital of Zhejiang Chinese Medical University, Hangzhou 310053, P.R. China*
[d]*School of Basic Medical Sciences, Zhejiang Chinese Medical University, Hangzhou 310053, P.R. China*
[e]*The Second Affiliated Hospital of Zhejiang Chinese Medical University, Hangzhou 310053, P.R. China*
†These authors have contributed equally to this work and share first authorship.

Open Access Article. Published on 09 September 2025. Downloaded on 1/11/2026 8:00:54 PM.
This article is licensed under a Creative Commons Attribution-NonCommercial 3.0 Unported Licence.

types—from characteristic erythematous eruptions and polyarticular involvement to the devastating nephritis, alopecia, and serositis that define this protean disease.[2] Contemporary therapeutic arsenals against SLE remain frustratingly inadequate, plagued by therapeutic ceilings and formidable toxicity profiles that underscore an urgent imperative for revolutionary interventions. Traditional Chinese Medicine (TCM) emerges as a beacon of therapeutic promise, wielding its ancient wisdom through sophisticated multi-target pharmacological orchestration to combat autoimmune pathology.

Network pharmacology emerges as a revolutionary interdisciplinary paradigm, seamlessly weaving together systems pharmacology, computational biology, and sophisticated data mining architectures to illuminate the labyrinthine interactions between bioactive compounds and their molecular targets.[3,4] Through elegant network topology algorithms, this cutting-edge approach unveils mechanistic intricacies with unprecedented clarity, establishing itself as an indispensable platform for therapeutic discovery and pathway elucidation, particularly within the enigmatic realm of TCM research. The present investigation harnesses a meticulously crafted target-centric strategy, deploying advanced reverse screening methodologies to systematically unveil bioactive compounds and their botanical origins, culminating in an exquisitely optimized therapeutic selection framework.

Glycyrrhizin (GL), an extraordinary triterpenoid saponin gracefully extracted from the venerable *Glycyrrhiza* species, has captivated scientific attention through its formidable anti-inflammatory and immunomodulatory prowess. At the molecular epicenter, GL operates as an exquisite antagonist of high mobility group box 1 (HMGB1), masterfully disrupting the deleterious molecular liaison between HMGB1 and nucleic acids.[5] This sophisticated inhibitory choreography profoundly neutralizes the aberrant immune tempest triggered by self-DNA recognition—a cardinal pathogenic cornerstone in SLE pathogenesis. Groundbreaking investigations employing lupus-prone murine paradigms have eloquently demonstrated GL's capacity to dramatically curtail circulating inflammatory cytokines, autoantibodies, and HMGB1 concentrations. Furthermore, GL orchestrates a remarkable suppression of macrophage hyperactivation while elegantly dismantling immune complex architecture, thereby achieving profound amelioration of lupus progression.[6,7] Nevertheless, the intricate molecular choreography underlying GL's therapeutic virtuosity in SLE demands comprehensive illumination.

The gut microbiome constitutes an extraordinarily complex and dynamic microbial cosmos, exquisitely orchestrating host physiological harmony through multifaceted regulatory networks. The preservation of microbial equilibrium represents a fundamental prerequisite for immune homeostasis, while its perturbation unleashes cascading pathological immune aberrations. In the SLE milieu, patients exhibit profound gut dysbiosis—a striking microbial catastrophe characterized by decimated commensal bacterial diversity and the ominous expansion of pathogenic microbial consortia.[8] This dysbiotic landscape devastates intestinal barrier integrity, creating pernicious conduits for bacterial translocation and the systemic dissemination of microbial antigens, thereby orchestrating a relentless amplification of inflammatory networks.[9] The dysregulation of specific microbial taxa exerts profound influence over immune cell fate determination and functional orchestration, further exacerbating the immunological chaos characteristic of SLE.[10,11] Moreover, perturbations in microbial metabolite profiles—particularly the depletion of short-chain fatty acids (SCFAs) and bile acid derivatives—have emerged as critical arbiters of host immune responses, wielding substantial influence over SLE pathogenetic trajectories.[12] GL demonstrates remarkable capacity to sculpt gut microbiota architecture,[13] potentially modulating these pivotal metabolic pathways and contributing to its therapeutic renaissance in SLE. However, the precise molecular orchestration mediating GL's microbiome-centric therapeutic symphony demands rigorous mechanistic exploration.

This investigation endeavors to illuminate the molecular pathways underlying GL's therapeutic magnificence in SLE through integrated bioinformatics virtuosity and meticulous *in vivo* experimental validation, unveiling mechanistic insights into its multi-target therapeutic mastery.

Materials and methods

Identification and integration of potential herbal targets for SLE

To acquire relevant target information for SLE, a thorough search was conducted using the keyword "systemic lupus erythematosus" across multiple databases: Genecards, OMIM, Drugbank, and Disgenet.[14–16] The retrieved target data were then standardized through the UniProt database.[17] Transformed target genes were subsequently imported into the Traditional Chinese Medicine Systems Pharmacology (TCMSP) database, where compounds interacting with these genes were identified retrospectively. These compounds underwent a rigorous screening process based on pharmacokinetic parameters (ADME) and Lipinski's rules.[18] The selection criteria included oral bioavailability (OB) of ≥30%, drug-likeness (DL) score of ≥0.18, and a drug half-life of >4 hours.[19] The curated data were then loaded into Cytoscape 3.7.2 software to construct a target-compound network.[20] Following this, the candidate compounds were aligned with corresponding herbal networks, facilitating the construction of a target-compound-herb network using Cytoscape 3.7.2's merge function module.

Molecular docking

Molecular docking was employed to predict interactions between target proteins and candidate compounds. The 3D structures of target proteins were obtained from the Protein Data Bank (PDB) and meticulously prepared by removing water molecules, adding hydrogen atoms, and optimizing the structures using appropriate force fields. Candidate compounds identified from the TCMSP database underwent optimization for docking, with their 3D structures generated and geometries

Open Access Article. Published on 09 September 2025. Downloaded on 1/11/2026 8:00:54 PM.
This article is licensed under a Creative Commons Attribution-NonCommercial 3.0 Unported Licence.

minimized using suitable algorithms and force fields. The prepared proteins and ligands were then subjected to molecular docking, wherein ligands were strategically placed into the binding sites of proteins and their binding affinities evaluated based on sophisticated scoring functions. Docking scores were computed to predict binding affinities, where lower scores indicated stronger predicted interactions. The docking results were subsequently validated through detailed visual inspection of binding poses.

Animals and treatments

4-Week-old female MRL/MpJ-Faslpr/J (MRL/lpr) mice and age-matched wild-type C57BL/6J female mice were purchased from Shanghai SLAC Laboratory Animal Co., Ltd (Shanghai, China) (n = 5 per experimental group). Mice were randomly assigned into four groups (*i.e.* normal control group, untreated MRL/lpr mice, low-dose glycyrrhizin-treated MRL/lpr mice, or high-dose glycyrrhizin-treated MRL/lpr mice). Glycyrrhizin (J&K Scientific, Shanghai, China), was administered *via* daily gavage for 4 weeks, with dosages set at 50 mg kg^{-1} for the low-dose group and 100 mg kg^{-1} for the high-dose group, as established in prior studies.[21,22] Throughout the study, animals had *ad libitum* access to food and tap water. Following the 4-week treatment period, the mice were euthanized using an overdose of pentobarbital sodium. Blood, feces, and kidney samples were collected for subsequent analysis. All experimental procedures adhered to the National Institutes of Health (NIH) guidelines for Laboratory Animal Care and were overseen and approved by the Institutional Animal Care and Use Committee of Zhejiang Chinese Medical University.

Enzyme-linked immunosorbent assay (ELISA)

Adhere meticulously to the protocol provided by the ELISA kit (Ruixin Biotech, China) to process serum samples and accurately quantify the concentrations of serum antinuclear antibodies (ANA) and anti-dsDNA.

Histopathological analysis

Upon obtaining the kidney tissue samples, they were immediately fixed in 10% formalin (Servicebio, China). The fixed tissues were then embedded in paraffin and sectioned into 3–5 μm thick slices using a microtome (Leica RM2235, Leica Biosystems, Germany). These sections were mounted on glass slides and dewaxed through sequential washes with xylene and ethanol (Sinopharm Chemical Reagent Co., China). For histological examination, sections were stained with hematoxylin and eosin (H&E; G1120, Solarbio, China) to evaluate general morphology, periodic acid-Schiff (PAS; G1281, Solarbio, China) to assess the basement membrane and mesangial matrix, and Masson's trichrome to identify fibrosis and collagen deposition (G1340, Solarbio, China). The stained slides were examined under an optical microscope (Olympus BX53, Japan), and images were captured for further analysis (DP80, Olympus, Japan). Image analysis software was utilized to perform quantitative measurements of parameters such as fibrosis extent and basement membrane thickening, providing a comprehensive understanding of the pathological status of the renal tissue. To quantitatively evaluate Masson's trichrome and PAS staining, images were acquired under consistent magnification, illumination, and exposure settings using a high-resolution automated imaging system to capture detailed staining features. Multiple non-overlapping, representative fields were randomly selected from each slide to comprehensively account for staining variations and tissue architecture. These regions were defined and analyzed using ImageJ (NIH, USA) and Image-Pro Plus software (Media Cybernetics, USA), with specific analysis parameters tailored to each staining type: Masson's trichrome staining was used to assess collagen and muscle fibers and PAS staining to evaluate glycogen and mucin. Each slide was independently reviewed by three blinded evaluators under standardized conditions to ensure scoring consistency and minimize bias. In cases of significant discrepancies, a re-evaluation process was conducted. The final data were averaged, and statistical analyses were performed to compare staining intensity and positive areas across experimental groups, providing objective and reproducible data for reliable inter-group comparisons.

16S rDNA sequencing

DNA extraction from different samples was performed using the CTAB DNA extraction kit (TIANGEN Biotech, Beijing, China) according to the manufacturer's instructions, which is effective for isolating DNA from trace amounts of sample and suitable for most bacterial DNA. Nuclear-free water was used as a blank control, and the total DNA was eluted in 50 μL of elution buffer and stored at −80 °C until PCR analysis. All PCR measurements were carried out at LC-Bio Technology Co., Ltd (Hangzhou, Zhejiang Province, China). The 5′ ends of the primers were tagged with specific barcodes unique to each sample along with sequencing universal primers. PCR amplification was performed in a total reaction volume of 25 μL, containing 25 ng of template DNA, 12.5 μL of PCR Premix (Vazyme, China), 2.5 μL of each primer, and PCR-grade water (Vazyme, China) to adjust the volume. The amplification conditions for prokaryotic 16S fragments included an initial denaturation at 98 °C for 30 seconds; followed by 32 cycles of denaturation at 98 °C for 10 seconds, annealing at 54 °C for 30 seconds, and extension at 72 °C for 45 seconds; and a final extension at 72 °C for 10 minutes. PCR products were confirmed on 2% agarose gel electrophoresis. Throughout the DNA extraction process, ultrapure water was used as a negative control to rule out false-positive PCR results. Purification of the PCR products was performed using AMPure XT beads (Beckman Coulter Genomics, Danvers, MA, USA), and quantification was completed with a Qubit fluorometer (Invitrogen, USA). Amplicon pools were prepared for sequencing, with library size and quantity assessed using the Agilent 2100 Bioanalyzer (Agilent, USA) and the Library Quantification Kit for Illumina (Kapa Biosciences, Woburn, MA, USA), respectively. Sequencing was conducted on the Illumina NovaSeq PE250 platform according to the manufacturer's recommendations by LC-Bio Technology Co., Ltd. Paired-end reads were

Open Access Article. Published on 09 September 2025. Downloaded on 1/11/2026 8:00:54 PM.
This article is licensed under a Creative Commons Attribution-NonCommercial 3.0 Unported Licence.

assigned to samples based on their unique barcodes and were processed by removing barcodes and primer sequences. Reads were merged using FLASH, and quality filtering was conducted using fqtrim (v0.94) to obtain high-quality clean tags. Chimeric sequences were filtered using Vsearch (v2.3.4). Dereplication was performed using DADA2, resulting in the final feature table and feature sequences.

GEO data validation analysis

The GEOquery package in R was employed to identify and acquire raw data from lupus nephritis-related datasets (GSE32592, GSE113342, and GSE112943). Integrity and consistency of the downloaded raw data files were ensured, followed by data standardization and quality control procedures to correct for technical variations and ensure comparability across samples. Differential expression analysis was then conducted to identify genes with significant expression differences between the blank control and lupus nephritis groups. The differentially expressed genes from the three datasets were integrated into a comprehensive gene set representing disease differential expression. Potential drug targets were identified by querying the drug target databases SEA, Superpred, and SwissTargetPrediction using the keyword "glycyrrhizin", and the identified targets were consolidated into a cohesive collection. A comparative analysis was conducted between the disease-related gene set and the identified drug targets to screen for overlapping genes. Enrichment analysis was then performed to identify overrepresented Gene Ontology (GO) terms and Kyoto Encyclopedia of Genes and Genomes (KEGG) pathways within the differentially expressed genes. Following the identification of the target pathway, a protein–protein interaction (PPI) network was constructed using the STRING database to explore the interactions and functional associations between the genes.

Immunofluorescence and immunohistochemistry analysis

Kidney tissues were harvested and fixed in 10% neutral buffered formalin (Servicebio, China). The fixed tissues were embedded in paraffin and sectioned into 4 μm slices (Leica RM2235, Leica Biosystems, Germany). Sections were dewaxed, rehydrated (Sinopharm Chemical Reagent Co., China), and subjected to antigen retrieval using citrate buffer (pH 6.0; Beyotime, Shanghai, China). To block endogenous peroxidase activity, sections were treated with 3% hydrogen peroxide (Beyotime, Shanghai, China), followed by blocking with 5% bovine serum albumin (BSA; Sigma-Aldrich, USA). Primary antibodies against PDGFRα, PDGFRβ, KDR (all from Cell Signaling Technology), and PKCα (UpingBio, China), were applied to the sections and incubated overnight at 4 °C. After washing, sections were incubated with biotinylated secondary antibodies (ZSGB-BIO, Beijing, China) and horseradish peroxidase (HRP)-conjugated streptavidin (ZSGB-BIO, Beijing, China). Detection was performed using diaminobenzidine (DAB; ZSGB-BIO, Beijing, China), followed by counterstaining with hematoxylin (Solarbio, Beijing, China). Sections were then dehydrated, cleared, and mounted for histological analysis. For immunofluorescence, sections were treated with fluorophore-conjugated secondary antibodies (Thermo Fisher Scientific, USA), counterstained with DAPI (Beyotime, China), and imaged using a fluorescence microscope (Olympus BX53, Olympus, Japan). Quantitative evaluation of immunofluorescence and immunohistochemical staining was performed on tissue sections, with specific regions of interest selected as described in the histopathological analysis. Different analysis parameters were applied: immunofluorescence staining was used to quantify the area and intensity of fluorescence-positive regions, while immunohistochemistry focused on segmenting positive areas and measuring their intensity. Consistent evaluation methods were employed to ensure objective and reproducible data, supporting comparative analysis between experimental groups.

Short-chain fatty acid analysis by GC-MS

To quantitatively determine the concentrations of SCFAs, specifically acetate and butyrate, in serum samples, gas chromatography-mass spectrometry (GC-MS) was employed. Serum proteins were precipitated using HPLC-grade methanol (Sigma-Aldrich, USA), followed by acidification with hydrochloric acid (37%, Merck, Germany), and extraction with *n*-butanol (Sigma-Aldrich, USA) to isolate target metabolites. The extracts were derivatized using *N-tert*-butyldimethylsilyl-*N*-methyltrifluoroacetamide (MTBSTFA, Sigma-Aldrich, USA) at 60 °C for 30 minutes to enhance volatility and detection sensitivity. The derivatized products were analyzed on an Agilent 7890B gas chromatograph coupled with a 5977B mass selective detector in selected ion monitoring (SIM) mode. Quantification was performed using calibration curves prepared with high-purity standards of acetate and butyrate (≥99%, Sigma-Aldrich). The method demonstrated excellent linearity (R^2 > 0.99), reproducibility, and recovery, and is suitable for high-throughput quantification of SCFAs in serum matrices.

Serum calcium concentration measurement

Serum Ca^{2+} levels were measured using an Arsenazo III-based assay kit (Nanjing Jiancheng, China). A 10 μL serum sample was reacted with the reagent at room temperature for 10 min, and absorbance was read at 650 nm using a microplate reader (BioTek, USA). Concentrations were calculated from a standard curve.

Serum LPS level determination

Serum LPS levels were quantified by ELISA using a mouse-specific kit (CUSABIO, China). Samples were incubated at 37 °C for 90 min in pre-coated plates, followed by washing, HRP-conjugate addition, and color development. Absorbance was measured at 450 nm, and concentrations were determined *via* standard curves.

Western blot analysis

The kidney samples were lysed in ice-cold RIPA buffer (Beyotime, China) supplemented with 1% PMSF (Beyotime,

Open Access Article. Published on 09 September 2025. Downloaded on 1/11/2026 8:00:54 PM.
This article is licensed under a Creative Commons Attribution-NonCommercial 3.0 Unported Licence.

China) and a protease inhibitor cocktail (Roche, Basel, Switzerland) for 30 minutes, with intermittent vortexing every 5 minutes to ensure thorough homogenization. Following lysis, the samples were centrifuged at 12 000*g* for 10 minutes at 4 °C, and the supernatant containing the total protein extract was collected. Protein concentrations were determined using the BCA Protein Assay Kit (Thermo Fisher Scientific, USA). Equal amounts of protein (20 μg per sample) were denatured by boiling at 95 °C for 5 minutes in 5× SDS loading buffer (Beyotime, China) and then resolved on SDS-PAGE gels (GenScript, Nanjing, China). Subsequently, proteins were transferred onto PVDF membranes (Millipore, USA). The membranes were blocked with 5% skim milk (BD Difco, USA) in TBST at room temperature for 1 hour to prevent nonspecific binding. Primary antibodies against PDGFRα, PDGFRβ, KDR (all from Cell Signaling Technology, USA), and PKCα (UpingBio, China) were applied, along with a β-actin antibody (Cell Signaling Technology, USA) as the internal control, and incubated overnight at 4 °C. The following day, after thorough washing with TBST, the membranes were incubated with HRP-conjugated secondary antibodies (Cell Signaling Technology, USA). Protein bands were visualized and quantified using the FluorChem FC3 imaging system (ProteinSimple, USA). Target proteins levels were normalized to β-actin. Each experiment was conducted in triplicate to ensure reproducibility.

Statistics

The experimental data are presented as mean ± standard deviation (SD). To evaluate the differences between the four experimental groups, a one-way analysis of variance (ANOVA) test was employed. Statistical significance was determined with a *P*-value < 0.05 (* <0.05, ** <0.01).

Results

Candidate compound acquisition and target-compound-herb network construction

In the preliminary phase of drug screening, we conducted a systematic analysis across multiple disease-specific databases

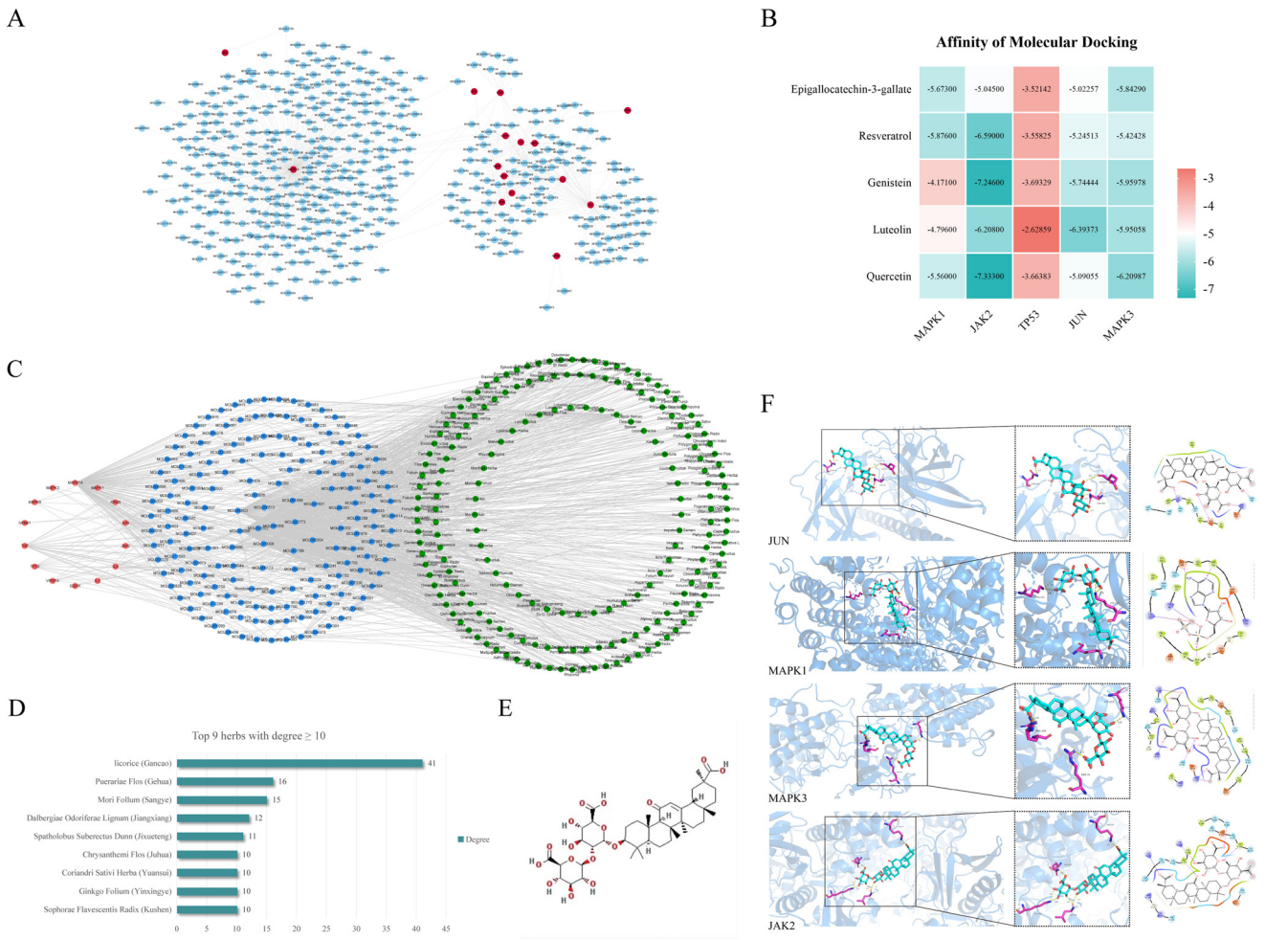

Fig. 1 Target-compound-herb network construction and glycyrrhizin identification. (A) Target-compound network. (B) Affinity of molecular docking. (C) Target-compound-herb network. (D) Distribution of herbs according to degree values. (E) Molecular structural formula of glycyrrhizin. (F) 3D presentation of molecular docking between glycyrrhizin and the hub genes.

Open Access Article. Published on 09 September 2025. Downloaded on 1/11/2026 8:00:54 PM.
This article is licensed under a Creative Commons Attribution-NonCommercial 3.0 Unported Licence.

to compile a comprehensive dataset encompassing 1560 potential SLE-related therapeutic targets (Material S1). Through network topology analysis, we identified 14 hub genes—including MAPK1, MAPK3, TP53, JUN, and JAK2—that demonstrated high degree centrality and were considered pivotal nodes in TCM-SLE therapeutic interactions. Following standardization of protein nomenclature *via* the UniProt database, we performed reverse screening against the TCMSP database, which yielded 167 compounds satisfying our predefined selection criteria (Material S2). These compounds were subsequently classified as key bioactive molecules. To elucidate the core molecular interactions, we constructed a Target-Compound network (Fig. 1A), revealing five principal candidate compounds: Genistein, Epigallocatechin-3-gallate, Luteolin, Quercetin, and Resveratrol. Molecular docking analyses demonstrated moderate to strong binding affinities between the majority of candidate compounds and their corresponding hub targets, with the notable exception of TP53, which exhibited relatively weak binding interactions (Fig. 1B). To establish the pharmacological context within traditional Chinese medicine frameworks, we employed reverse mapping to trace the 167 key compounds to their botanical origins using the TCMSP database, identifying 473 medicinal species. Frequency analysis revealed 196 herbs associated with a minimum of 10 candidate compounds (Material S3). Subsequently, we constructed a comprehensive Target-Compound-Herb network to delineate the intricate relationships among therapeutic targets, bioactive compounds, and their herbal sources (Fig. 1C).

Notably, Licorice (*Glycyrrhiza uralensis*) emerged as the most pharmacologically significant herb within this network, demonstrating the highest frequency of associations with both key compounds (n = 41) and target interactions, thereby establishing its central role in the TCM-based anti-SLE therapeutic landscape[23] (Fig. 1D). Among its bioactive constituents, Glycyrrhizin (GL, Fig. 1E) was recognized as the predominant compound, characterized by extensively documented immunomodulatory and anti-inflammatory properties.[24] While GL was not initially ranked among the top candidate compounds based solely on hub-target affinity analysis, it was prioritized for subsequent investigation based on two critical rationales: (1) its status as the primary bioactive constituent of licorice—the most enriched herb in our compound-herb mapping analysis, and (2) its high-frequency association with multiple hub targets through reverse screening. Confirmatory molecular docking studies demonstrated robust binding affinities between GL and all prioritized targets except TP53, thereby validating its therapeutic potential (Fig. 1F).

Glycyrrhizin ameliorated immune levels and renal pathology in MRL/lpr mice

The therapeutic potential of GL was systematically assessed in the MRL/lpr murine model of systemic lupus erythematosus (Fig. 2A). Administration of GL across a spectrum of dosages elicited remarkable amelioration of immunological dysregulation, manifested through substantial suppression of pathogenic autoantibodies, including ANA and anti-dsDNA—cardinal biomarkers of aberrant immune hyperactivation characteristic of lupus pathogenesis. Particularly noteworthy was the superior therapeutic response observed in the high-dose cohort, which demonstrated the most pronounced immunomodulatory effects (Fig. 2B).

Histopathological examination of renal architecture provided compelling corroborative evidence of GL's therapeutic efficacy, revealing dose-dependent amelioration of nephritis pathology characterized by marked attenuation of inflammatory cellular infiltrates, substantial resolution of glomerular lesions, notable regression of basement membrane thickening, and significant mitigation of interstitial fibrosis. Immunofluorescence microscopy unveiled a striking reduction in glomerular immune complex deposition following GL intervention (Fig. 2C), with the most dramatic improvements manifested in the high-dose treatment group—findings that exhibited remarkable concordance with the observed diminution in circulating autoantibody titers.

Glycyrrhizin modulated the gut microbiota composition in MRL/lpr mice

GL has been previously reported to modulate gut microbiota composition.[13] Given the recognized contribution of gut dysbiosis to the immunopathogenesis of SLE, we performed 16S rDNA high-throughput sequencing of cecal contents from MRL/lpr mice across distinct treatment groups to comprehensively delineate microbial structural and compositional dynamics. Sequencing results revealed 304 shared amplicon sequence variants (ASVs) and 5344 unique ASVs, with 1813, 1123, 1238, and 1170 uniquely detected in the control, model, low-dose GL, and high-dose GL groups, respectively (Fig. 3A). Following data normalization, α- and β-diversity analyses were conducted. While α-diversity indices showed no statistically significant differences in species richness or evenness across groups (Fig. 3B), β-diversity analysis *via* principal coordinate analysis (PCoA) demonstrated clear separation between groups, indicating a marked reshaping of microbial community structures (Fig. 3C).

At the phylum level, the microbiota was dominated by Firmicutes, Bacteroidota, Actinobacteriota, Verrucomicrobiota, and Proteobacteria (Fig. 3D). The Firmicutes/Bacteroidota (F/B) ratio was notably decreased in the model group, consistent with a shift toward a proinflammatory microbial phenotype previously associated with lupus.[25] Interestingly, low-dose GL administration elevated the F/B ratio, indicating a partial restoration of microbial homeostasis, whereas high-dose GL induced a slight but non-significant decline (Fig. 3E), implying a potential dose-dependent, non-linear modulatory effect.

At the genus level, detailed taxonomic profiling uncovered profound compositional disturbances in the model group (Fig. 3F). Genera associated with fiber degradation (Candidatus Saccharimonas, Eubacterium xylanophilum group, Robinsoniella), SCFA biosynthesis (Bacteroidales, Clostridia, Veillonella), and mucosal immune modulation

 This journal is © The Royal Society of Chemistry 2025

Open Access Article. Published on 09 September 2025. Downloaded on 1/11/2026 8:00:54 PM.
This article is licensed under a Creative Commons Attribution-NonCommercial 3.0 Unported Licence.

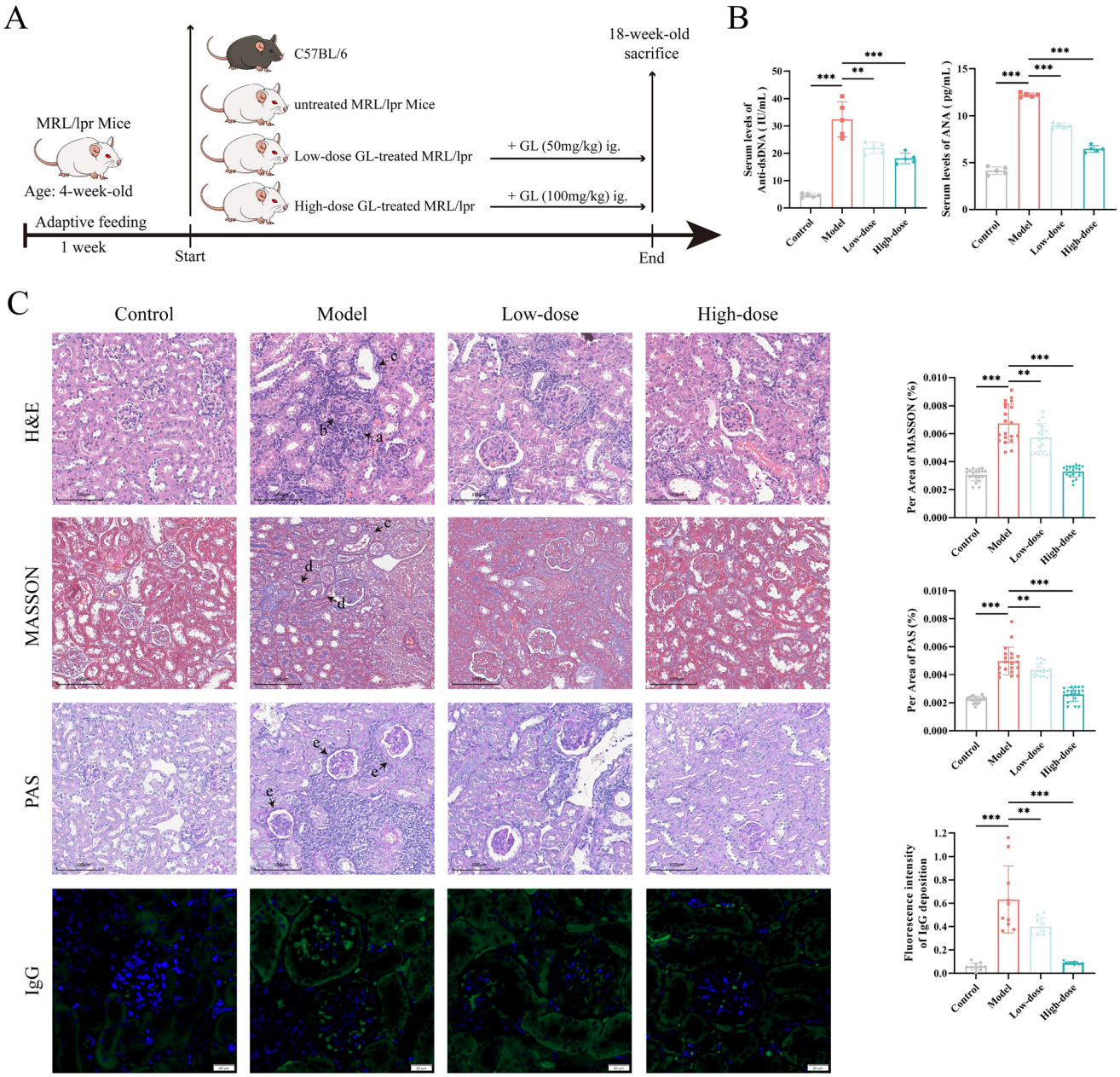

Fig. 2 Glycyrrhizin ameliorates disease severity in MRL/lpr Mice. (A) Animal experiment flowchart. (B) The levels of serum ANA and anti-dsDNA. Each group consisted of 5 samples (n = 5 per group). (C) Representative images of H&E, Masson trichrome, and PAS staining from each group (scale bar: 100 μm), along with high-resolution images of mouse IgG immunofluorescence staining (scale bar: 20 μm). In the H&E-stained sections, the following pathological features were annotated: a, infiltration of inflammatory cells; b, glomerular hyperplasia and sclerosis; c, tubular dilatation and atrophy. In the Masson-stained sections, d, indicates fibrotic collagen deposition; in the PAS-stained sections, e, denotes thickening of the glomerular basement membranes. Semi-quantitative analyses are provided alongside. Each group contained three biological replicates (n = 3 per group). Data are presented as the mean ± SD. Statistical significance is denoted as *P < 0.05, **P < 0.01 *versus* the model group.

were significantly diminished (Fig. 3G), suggestive of impaired fermentative and immunoregulatory functions.[26–28] Conversely, opportunistic or proinflammatory genera including Tyzzerella, Dorea, Helicobacter, Anaeroplasma, and Pseudoflavonifractor were enriched, aligning with microbial signatures known to potentiate intestinal permeability, metabolic dysregulation, and host immune activation.[29–31] GL administration effectively reversed many of these compositional aberrations, suggesting robust microbiota-targeted pharmacological effects. Given the documented association between *Ruminococcus* and SLE disease activity and renal involvement,[32,33] we specifically examined its abundance. LEfSe analysis (Fig. 3H) and subsequent quantification revealed a significant elevation of *g_Ruminococcus* and *s_Ruminococcus_unclassified* in the model group, which was dose-dependently attenuated following GL treatment (Fig. 3I

Open Access Article. Published on 09 September 2025. Downloaded on 1/11/2026 8:00:54 PM.
This article is licensed under a Creative Commons Attribution-NonCommercial 3.0 Unported Licence.

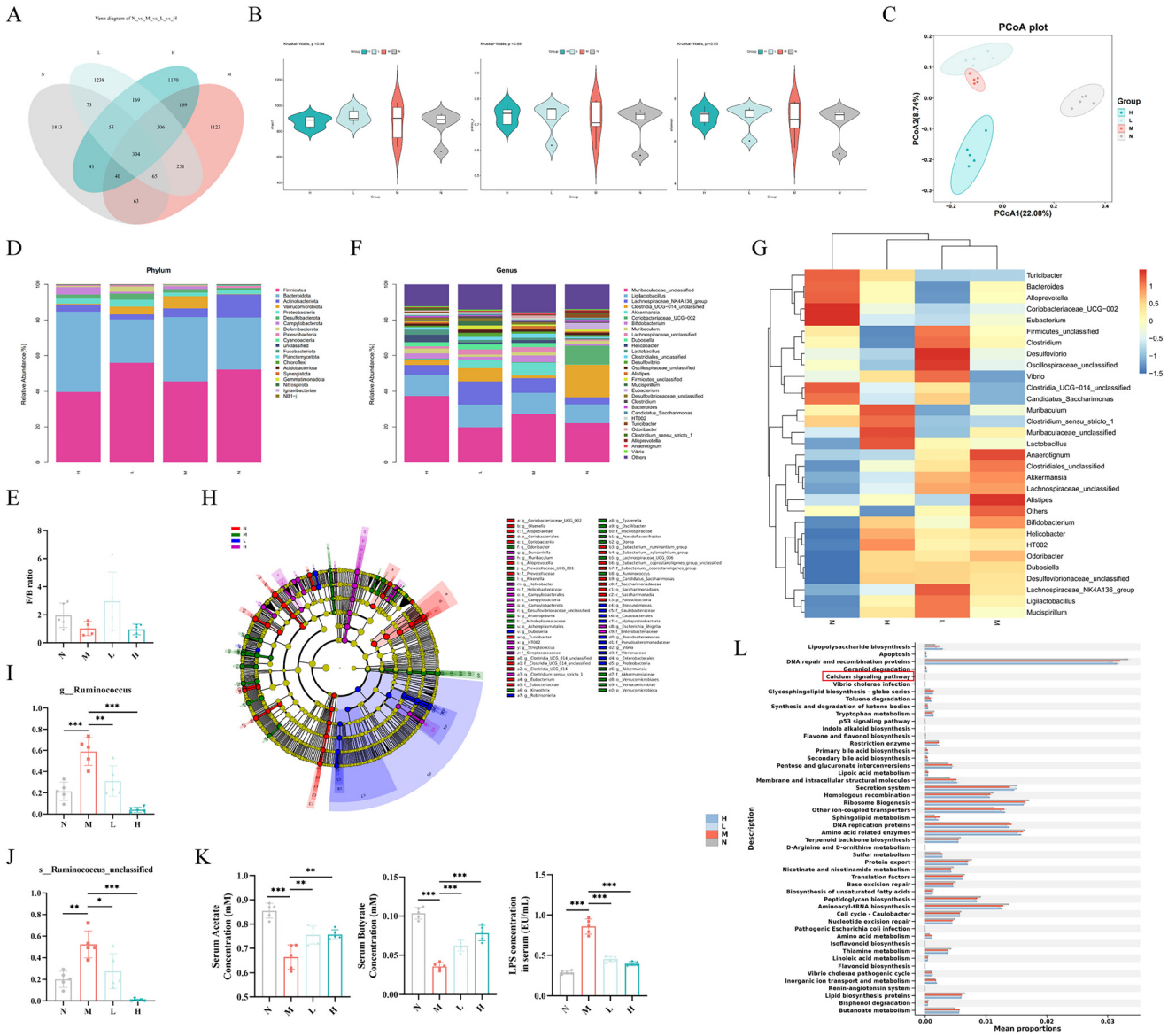

Fig. 3 Glycyrrhizin modulated the gut microbiota composition. (A) Venn diagram showing the distribution of shared and unique ASVs across groups. (B) Violin plots illustrating the alpha diversity indices comparison. (C) The PCoA plot displaying the distribution along the first two principal coordinates (PCoA1 and PCoA2). (D) Stacked bar chart displaying the relative abundance of microbial communities at the phylum level across the different groups. (E) The Firmicutes/Bacteroidota (F/B) ratio in each group. (F) Stacked bar chart displaying the relative abundance of microbial communities at the genus level. (G) Heatmap showing the hierarchical clustering of the top 30 microbial communities with relative abundance at the genus level. (H) LEfSe analysis identifying dominant bacterial species. (I and J) The relative abundance of the *g_Ruminococcus* and *s_Ruminococcus_unclassified*. (K) Serum concentrations of acetate, butyrate, and LPS. (L) Presentation of PICRUSt2-based functional predictions. Each group consisted of 5 samples (n = 5 per group). Data are presented as the mean ± SD. Statistical significance is denoted as $^{*}P < 0.05$, $^{**}P < 0.01$ *versus* the model group (N: control; M: model; L: low-dose GL; H: high-dose GL).

and J). This targeted microbial suppression may represent a mechanistic axis by which GL alleviates lupus severity.

To functionally validate the physiological relevance of these microbiota shifts, we quantified serum levels of two major SCFAs—acetic acid and butyric acid—as well as lipopolysaccharide (LPS), a marker of gut-derived endotoxemia (Fig. 3K). In the model group, both SCFAs were markedly reduced, reflecting compromised microbial fermentation capacity, while LPS levels were significantly elevated, indicating increased intestinal permeability and systemic inflammatory burden. GL treatment restored SCFA concentrations and significantly suppressed LPS levels in a dose-dependent manner.

Complementing these biochemical findings, PICRUSt2-based metagenomic prediction exposed pronounced, group-specific enrichment of several functional pathways (Fig. 3L). Most notably, the calcium-signaling pathway—a nexus previously implicated in lupus nephritis pathogenesis—was preferentially enriched. In addition, pathways involved in lipopo-

This journal is © The Royal Society of Chemistry 2025

Open Access Article. Published on 09 September 2025. Downloaded on 1/11/2026 8:00:54 PM.
This article is licensed under a Creative Commons Attribution-NonCommercial 3.0 Unported Licence.

lysaccharide biosynthesis, amino-acid and lipid metabolism, and DNA repair/recombination were dysregulated in diseased mice but shifted following GL administration.

Collectively, these results demonstrate that GL exerts a nuanced, dose-responsive regulatory influence on the gut microbial ecosystem in MRL/lpr mice. By restoring taxonomic equilibrium, enhancing SCFA output, and curbing endotoxemia, GL contributes to the re-establishment of intestinal and systemic immune homeostasis.

Investigation on molecular mechanisms of glycyrrhizin in LN treatment based on GEO database

Given the pronounced intergroup heterogeneity in *g_Ruminococcus* abundance and its established implication in LN pathogenesis, we postulated a mechanistic nexus between GL-induced microbiome alterations and renal immunoregulatory cascades. To comprehensively delineate the putative molecular substrates, we amalgamated transcriptomic profiles from

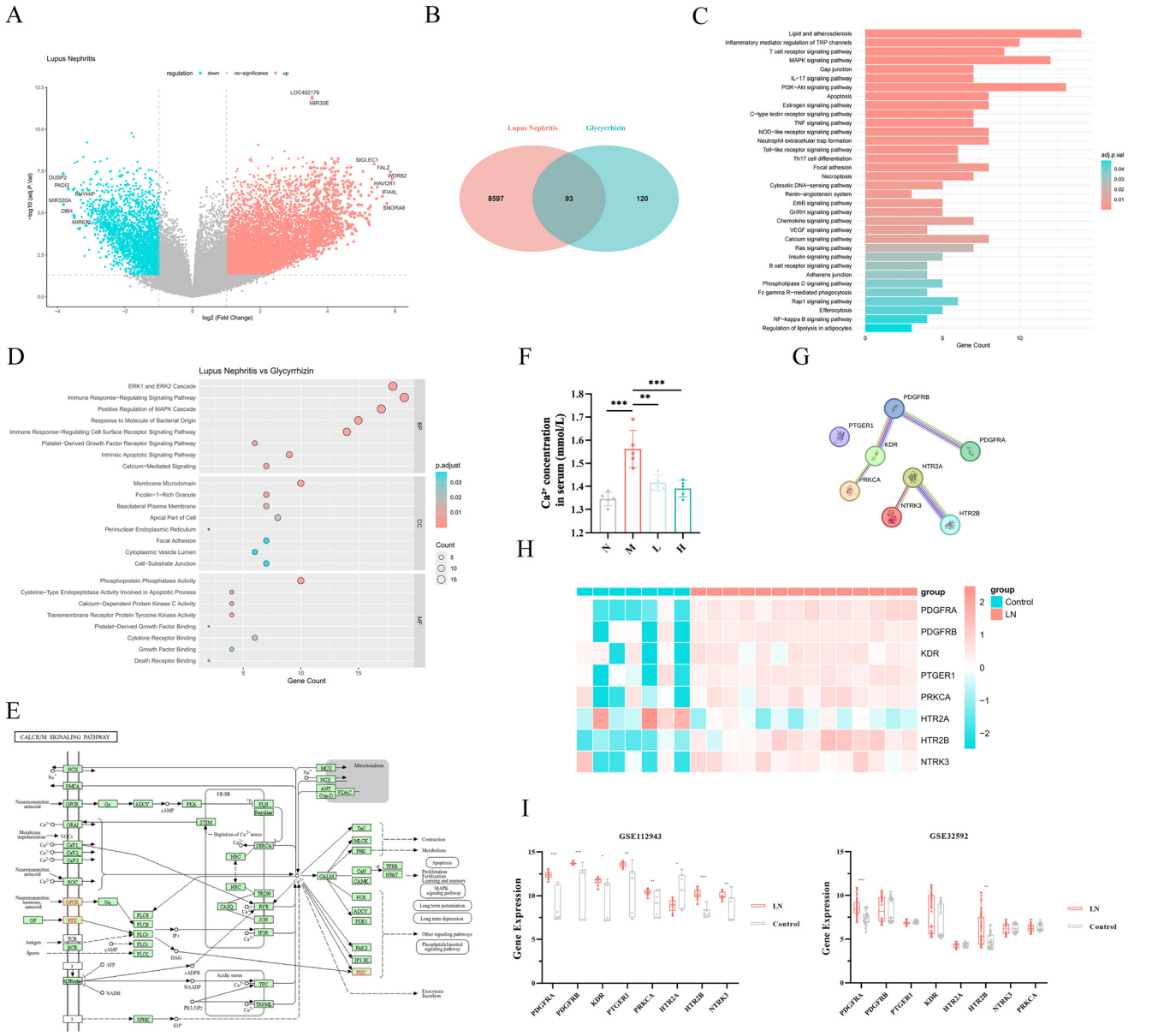

Fig. 4 Investigation on molecular mechanisms of glycyrrhizin in LN treatment based on GEO database. (A) Volcano plot displaying the integrated distribution of DEGs. Red dots represent upregulated genes, while blue dots represent downregulated genes. (B) Intersection between integrated DEGs and GL-associated targets. (C and D) KEGG and GO enrichment analyses. (E) Detailed calcium signaling pathway map. The protein highlighted in red indicates increased expression in the model group. (F) Serum concentrations of Ca^{2+}. (G) PPI network of genes identified in calcium signaling pathway. (H) The expression levels of key DEGs after integration. (I) The expression levels of key DEGs from individual datasets. Data are presented as the mean ± SD. Statistical significance is denoted as $*P < 0.05$, $**P < 0.01$ *versus* the model group (N: control; M: model; L: low-dose GL; H: high-dose GL).

Open Access Article. Published on 09 September 2025. Downloaded on 1/11/2026 8:00:54 PM.
This article is licensed under a Creative Commons Attribution-NonCommercial 3.0 Unported Licence.

three LN-associated datasets (GSE32592, GSE113342, and GSE112943) procured from the Gene Expression Omnibus (GEO) repository (Fig. 4A). Concurrently, GL-associated molecular targets were systematically curated from the SEA, SuperPred, and SwissTargetPrediction platforms. Bioinformatic cross-interrogation of these repositories unveiled 93 convergent genetic loci, delineating a cohort of GL targets putatively implicated in LN pathogenesis (Fig. 4B). Ensuing pathway enrichment analyses *via* KEGG and GO frameworks of the convergent genetic entities revealed conspicuous enrichment within the

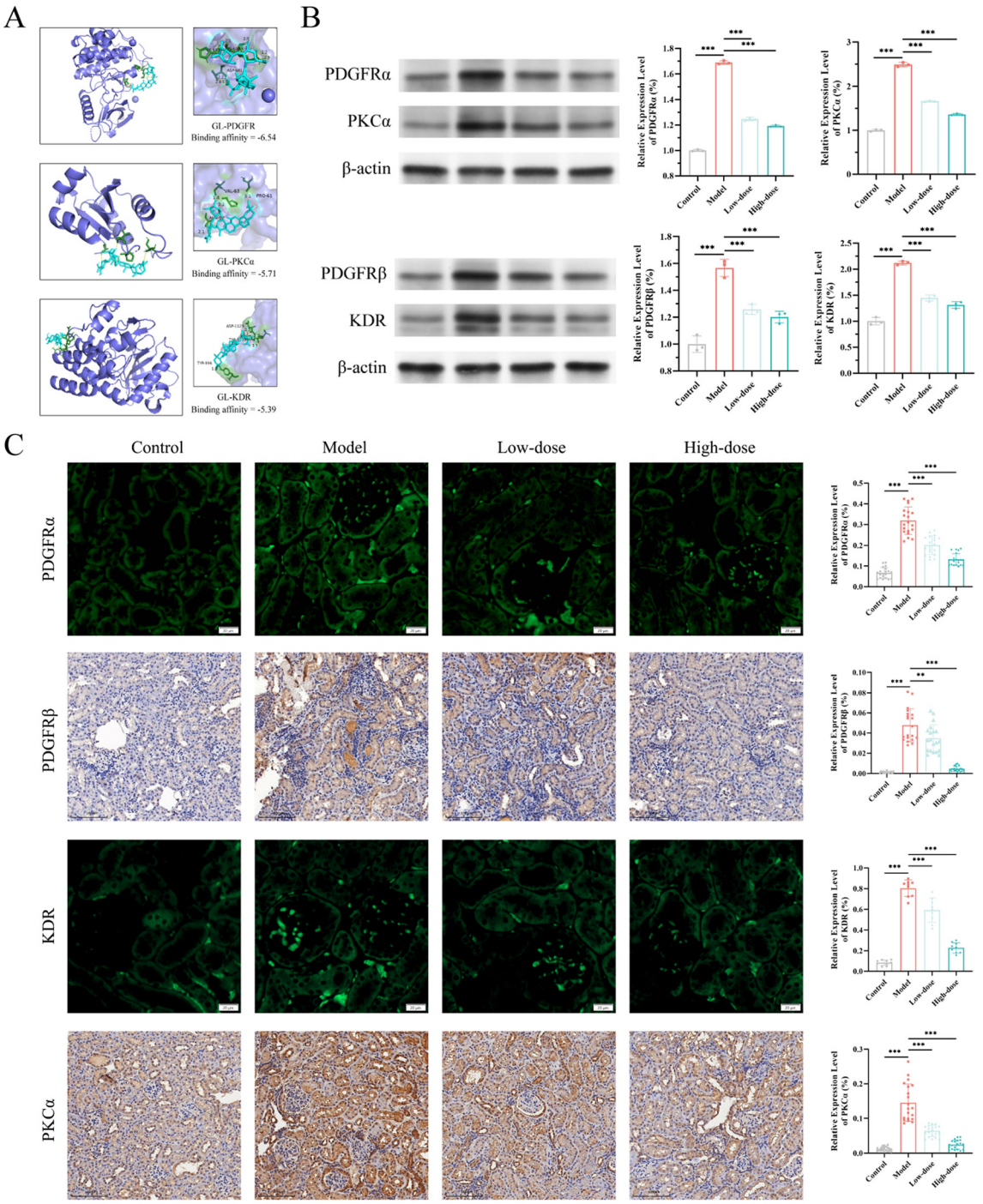

Fig. 5 Glycyrrhizin suppressed the renal RTK-PKC axis activation. (A) Molecular docking interactions between glycyrrhizin and key targets (PDGFR, KDR, and PKCα). (B) Western blot analysis with corresponding quantification. Each group consisted of 3 samples (n = 3 per group). (C) Representative fluorescence staining images of PDGFRα and KDR across groups (scale bar: 20 μm), along with detailed immunohistochemistry images of PDGFRβ and PKCα (scale bar: 100 μm), supplemented by comprehensive semi-quantitative analysis. Each group consisted of 3 samples (n = 3 per group). Data are presented as the mean ± SD. Statistical significance is denoted as *P < 0.05, **P < 0.01 *versus* the model group.

Open Access Article. Published on 09 September 2025. Downloaded on 1/11/2026 8:00:54 PM.
This article is licensed under a Creative Commons Attribution-NonCommercial 3.0 Unported Licence.

calcium signaling pathway (Fig. 4C–E). Remarkably, this finding corroborated the functional inferences extrapolated from 16S rDNA-based microbiotal analysis (see Fig. 3L), thus substantiating that the calcium signaling axis may constitute a convergent mechanistic nexus bridging intestinal dysbiosis and nephropathological manifestations.

To corroborate this postulate, we quantified circulating calcium concentrations across experimental cohorts. Notably, serum calcium levels were profoundly perturbed in the pathological group relative to controls and were systematically reconstituted following GL intervention (Fig. 4F), intimating that microbiota-orchestrated perturbations may modulate systemic calcium equilibrium. These observations substantiate the proposition that calcium ions may function as a molecular conduit linking intestinal microbiotal alterations with downstream renal signaling cascades. A comprehensive mechanistic blueprint of the calcium signaling architecture was subsequently reconstructed, incorporating transcriptomic signatures to annotate pathway constituents. Notably, the PLCγ signaling module exhibited conspicuous activation, wherein receptor tyrosine kinases (RTKs) including PDGFRA, PDGFRB, and KDR demonstrated marked upregulation and orchestrated downstream PKC activation (Fig. 4E). Protein–protein interaction (PPI) network analysis further delineated PDGFRA, PDGFRB, KDR, and PKCA as cardinal nodes (Fig. 4G), substantiating their putative roles as principal effectors within this signaling framework. Transcriptomic profiles validated pronounced upregulation of calcium signaling-associated genes within the pathological cohor. Particularly, PDGFRA, PDGFRB, KDR, and PKCA exhibited distinctive yet convergent transcriptomic signatures indicative of their mechanistic engagement (Fig. 4H and I).

Collectively, these data substantiate that GL may orchestrate gut–renal crosstalk through reconstitution of microbiota-derived metabolites and normalization of systemic calcium signaling cascades.

Glycyrrhizin suppressed the renal RTK-PKC axis activation

Therefore, we interrogated the expression profiles of cardinal proteins implicated in the RTK-PKC signaling axis, as delineated in this investigation, within renal parenchyma. According to molecular docking simulations, GL demonstrated pronounced binding affinities with PDGFR, KDR, and PKCα (Fig. 5A). Western blot analysis unveiled conspicuous upregulation of PDGFRα, PDGFRβ, and KDR within the groups, which was dose-dependently attenuated following GL intervention, with the high-dose regimen exhibiting superior therapeutic efficacy. Concurrently, the downstream effector PKCα manifested elevated expression within the pathological group, which was substantially normalized upon GL administration (Fig. 5B). Immunofluorescence and histochemical analyses corroborated these observations, delineating a concordant expression pattern (Fig. 5C). These data illuminate GL's capacity to orchestrate therapeutic modulation of LN pathogenesis through targeted intervention at critical nodes within the calcium signaling cascade, particularly *via* suppression of PDGFRα, PDGFRβ, and KDR within the RTK pathway, alongside their downstream effector PKCα.

Discussion

Accumulating evidence underscores that the integration of TCM in SLE management has witnessed remarkable therapeutic advancement, with network pharmacology methodologies providing an unprecedented framework for identifying efficacious therapeutic entities. In this investigation, disease-associated molecular targets including MAPK1, MAPK3, TP53, JUN, and JAK2 were delineated as cardinal mediators in SLE pathogenesis. Specifically, MAPK1 and MAPK3 orchestrate T cell subset differentiation and clonal expansion, thereby amplifying systemic inflammatory cascades and representing putative biomarkers for LN.[34,35] Polymorphic variants and aberrant expression of TP53 are intrinsically linked to excessive keratinocyte proliferation, epidermal atrophy, and widespread apoptotic events characteristic of discoid lupus erythematosus (DLE).[20,36] JUN exhibits pronounced overexpression in SLE patient T cells following inflammatory stimulation, precipitating splenic tyrosine kinase (SYK) upregulation and T cell receptor activation, thereby facilitating lymphocytic infiltration and inflammatory amplification.[37] Furthermore, JAK2 primarily orchestrates inflammation and organ-specific pathological remodeling through downstream STAT protein activation, heightening T cell responsiveness to pro-inflammatory mediators.[38,39] Diverging from conventional network pharmacological paradigms, this study employed reverse-engineering strategies to identify candidate compounds targeting these pivotal disease mediators, subsequently validating molecular interactions through computational docking analyses to ascertain binding propensities. Comprehensive exploration of phytochemical origins revealed licorice (Gancao) as an exceptionally promising therapeutic entity. GL, the principal bioactive constituent of licorice, demonstrated substantial pharmacological potential, corroborated not only by precedent experimental evidence but also through confirmed interactions with SLE-associated targets exhibiting favorable binding characteristics. These findings provide robust theoretical underpinnings for GL's broad-spectrum regulatory capabilities, substantiating its selection as the primary compound for subsequent experimental validation and highlighting its therapeutic potential in SLE management.

In vivo validation further substantiated GL's therapeutic efficacy in MRL/lpr murine models. GL administration elicited significant attenuation of ANA and anti-dsDNA antibody concentrations, thereby ameliorating immunological dysregulation. Notably, GL markedly suppressed inflammatory cellular infiltration and glomerular pathological alterations within renal parenchyma. This investigation represents the first systematic demonstration of GL's dose-dependent therapeutic effects across varying concentrations, with high-dose regimens exhibiting particularly pronounced improvements in nephropathological parameters. Moreover, GL remarkably diminished

Open Access Article. Published on 09 September 2025. Downloaded on 1/11/2026 8:00:54 PM.
This article is licensed under a Creative Commons Attribution-NonCommercial 3.0 Unported Licence.

immune complex deposition within glomerular structures, concordant with its suppressive effects on autoimmune responses, thus reinforcing its therapeutic potential in SLE management.

Gut microbiotal exploration provides profound mechanistic insights into GL's systemic therapeutic effects in SLE. This study identified pronounced enrichment of *Ruminococcus genus* within the pathological cohort's intestinal microbiota. GL administration across varying dosages demonstrated significant modulation of *Ruminococcus* abundance, with notable reduction in relative prevalence. At refined taxonomic resolution, we identified unclassified bacterial species exhibiting similar perturbation patterns. This observation is particularly intriguing given prior research indicating that while *Ruminococcaceae* family generally exhibits diminished abundance in SLE patients' gut microbiota,[40–42] *Ruminococcus genus*, especially *Ruminococcus gnavus* (*R. gnavus*), demonstrates marked increased relative abundance.[43] *R. gnavus* has been implicated in cross-reactivity with native DNA, triggering anti-dsDNA antibody production—a pathognomonic hallmark of SLE pathology.[44] Furthermore, this species confirmes prominent association with renal impairment, with over 50% of active LN patients exhibiting *R. gnavus* expansion during disease exacerbation periods.[33] *R. gnavus* abundance alterations modulate immunoglobulin levels (IgG, IgM, IgA), contributing to intestinal barrier disruption, as evidenced by elevated fecal calprotectin, serum soluble CD14, and alpha-1-acid glycoprotein concentrations in SLE patients.[9] Notably, under specific clinical conditions—particularly when SLEDAI scores exceed threshold values of 8—conserved *R. gnavus* proteases exhibit pronounced reactivity with serum IgG antibodies, inducing robust strain-specific antibody responses.[32] In landmark investigations by Gregg J. Silverman and colleagues, a highly reactive *R. gnavus* subtype, RG2, was characterized, demonstrating significant reactivity in SLE patients, particularly those with nephritis, with RG2-specific antibody levels correlating closely with SLEDAI scores, autoantibody titers, serum complement levels, and inflammatory cytokine profiles.[9,32] Additionally, *R. gnavus* modulates T cell responses, particularly affecting regulatory T cell (Treg) populations,[45] and exhibits distinctive immunophenotypic regulation of B cell superantigen activity.[46] In lupus-prone murine models, including MRL/lpr and PIL mice—both recapitulating key human SLE features—*R. gnavus* relative abundance is similarly elevated,[43,47] mirroring genus-level observations in this study. Although this investigation did not delineate specific *Ruminococcus* subtype abundances, genus-level alterations observed indicate trends closely aligned with lupus pathogenesis and associated nephropathological complications. These findings suggest GL may exert therapeutic efficacy in SLE through gut microbiotal modulation, *via Ruminococcus genus* compositional alterations, thus modulating immune responses and ameliorating renal pathology.

Based on bioinformatics analysis utilizing GEO database resources, we further interrogated potential mechanisms underlying GL's therapeutic effects on LN. Our findings revealed that calcium signaling pathways, identified through enrichment analysis, corroborate gut microbiotal functional predictions. Refined mechanistic illustration suggests GL may modulate the RTK-PKCα axis, contributing to its therapeutic efficacy. The RTK family comprises an extensive and diverse group of receptor enzymes initiating signal transduction upon activation. In our study, PDGFRα and PDGFRβ, both PDGFR family tyrosine kinase members, were identified. Pathological PDGFR signaling activation predominantly drives excessive fibroblast proliferation and collagen overproduction, promoting fibrotic disease progression.[48,49] KDR (VEGFR2), a VEGFR family subtype, was also identified; its hyperactivation precipitates aberrant angiogenesis, resulting in glomerular capillary lesions and glomerulosclerosis, while increasing vascular permeability and disrupting glomerular filtration barriers.[50–52] Additionally, excessive VEGFR activation correlates with renal fibrosis progression.[53,54] In our study, PDGFRα, PDGFRβ, and VEGFR2 expression levels were substantially elevated in both glomerular and tubular compartments within the pathological cohort, with GL treatment effectively suppressing this upregulation, confirming GL's capacity to inhibit pathological RTK activation. RTK activation triggers PLCγ pathway activation, leading to phosphatidylinositol 4,5-bisphosphate (PIP2) hydrolysis into inositol trisphosphate (IP3) and diacylglycerol (DAG). IP3 subsequently facilitates calcium ion release from endoplasmic reticulum stores, which, in concert with DAG, activates PKC.[55] PKC, a critical serine/threonine kinase, can potentiate angiotensin II (Ang II) effects in glomerular compartments, causing vascular smooth muscle contraction and altering local hemodynamic parameters, ultimately resulting in increased glomerular filtration rate (GFR) and proteinuria onset.[56,57] Moreover, PKC activation upregulates vascular endothelial growth factor (VEGF) expression,[58] exacerbating vascular permeability and disrupting tubule-glomerular feedback mechanisms, further aggravating pathological progression. In renal tubular compartments, PKC activation induces pro-inflammatory cytokine expression, modulates TGF-β signaling, promotes extracellular matrix (ECM) production, and inhibits matrix metalloproteinase (MMP) activity, thereby impairing ECM remodeling and accelerating renal fibrosis.[59–61] PKCα, identified in this study, represents one of the most extensively expressed and comprehensively studied conventional PKC subfamily members.[62,63] In the model group, PKCα expression was markedly elevated in both glomerular and tubular compartments, whereas GL treatment suppressed this pathological activation. Thus, our study validates GL's regulatory role on the RTK-PKCα axis, particularly through significant downregulation of key targets following dose-dependent GL treatment, providing novel mechanistic insights into GL's therapeutic potential.

The glycyrrhizin dosing paradigm employed in this investigation (50 and 100 mg kg^{-1}) represents a meticulously calibrated therapeutic window that harmonizes with established efficacious ranges documented across diverse murine inflammatory models.[64–67] Through rigorous application of the FDA-endorsed body surface area conversion methodology (K_m factor approach), our dosing architecture translates to a human equivalent dose of 4.1–8.1 mg kg^{-1} day^{-1}, yielding a daily thera-

Open Access Article. Published on 09 September 2025. Downloaded on 1/11/2026 8:00:54 PM.
This article is licensed under a Creative Commons Attribution-NonCommercial 3.0 Unported Licence.

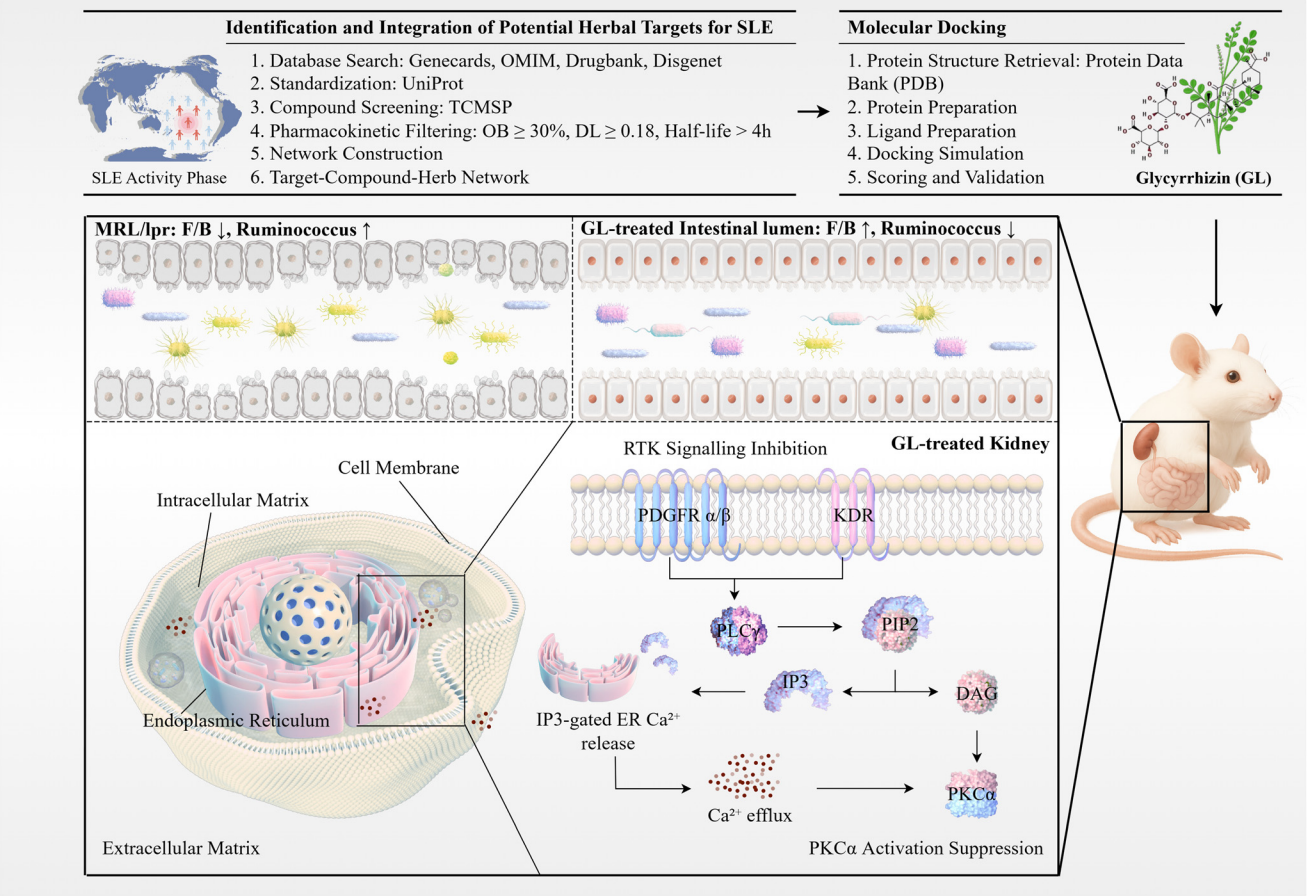

Fig. 6 Diagram illustrating a proposed mechanism by which glycyrrhizin alleviates renal damage in MRL/lpr mice by modulating gut microbiota dysbiosis and regulating the RTK-PKCα axis.

peutic range of 246–486 mg for a standard 60 kg adult. This dosing framework demonstrates remarkable congruence with internationally recognized safety benchmarks, residing comfortably within the 500 mg day^{-1} threshold established by both the World Health Organization and European Food Safety Authority as the upper boundary for minimizing glycyrrhizin-associated adverse manifestations, including electrolyte dysregulation and cardiovascular perturbations.[68,69] Our findings thus orchestrate a compelling translational narrative, whereby therapeutic efficacy converges seamlessly with established safety margins, creating an optimal foundation for clinical advancement. This sophisticated dosing strategy exemplifies the paradigmatic balance between pharmacological potency and patient safety, positioning glycyrrhizin as an exceptionally promising therapeutic candidate for chronic inflammatory disorders such as SLE, with unprecedented potential for seamless bench-to-bedside translation.

Conclusion

In synthesis, this investigation, through comprehensive multidimensional and multilayered analytical approaches, has substantively augmented experimental validation rigor and pioneered elucidation of glycyrrhizin's therapeutic paradigm in SLE and its nephropathological sequelae. The findings substantiate that glycyrrhizin may orchestrate its therapeutic efficacy through systematic modulation of intestinal microbiotal architecture, thereby regulating the RTK-PKCα signaling axis within calcium-mediated pathways, culminating in profound amelioration of renal pathological deterioration (Fig. 6). These discoveries furnish compelling experimental substantiation positioning glycyrrhizin as a promising therapeutic entity for SLE management, particularly in lupus nephritis intervention, and establish a robust conceptual framework for advancing more efficacious therapeutic paradigms in future clinical applications.

Author contributions

Fugang Huang: conceptualization, formal analysis, methodology, writing – original draft and writing – review & editing. Ke Sun: conceptualization, formal analysis, investigation, writing – original draft and writing – review & editing. Lijia Diao: data curation and formal analysis. Keda Lu: software and

Open Access Article. Published on 09 September 2025. Downloaded on 1/11/2026 8:00:54 PM.
This article is licensed under a Creative Commons Attribution-NonCommercial 3.0 Unported Licence.

resources. Yongsheng Fan: funding acquisition and writing – review & editing. Guanqun Xie: software, resources, supervision, funding acquisition and writing – review & editing. All authors contributed to the article and approved the submitted version. Yongsheng Fan and Guanqun Xie are responsible for the overall content as guarantor.

Data availability

The original contributions presented in the study are included in the article. Detailed data are available in the SI. Further inquiries are available by contact with the corresponding author.

Supplementary information is available. See DOI: https://doi.org/10.1039/d5fo01743b.

Conflicts of interest

The authors declare that they have no conflicts of interest.

Acknowledgements

Figdraw provides important graphic resources that contribute to better readability.

References

1 S. Lazar and J. M. Kahlenberg, Systemic lupus erythematosus: new diagnostic and therapeutic approaches, *Annu. Rev. Med.*, 2023, **74**, 339–352, DOI: 10.1146/annurev-med-043021-032611.
2 M. Kiriakidou and C. L. Ching, Systemic lupus erythematosus, *Ann. Intern. Med.*, 2020, **172**, ITC81–ITC96, DOI: 10.7326/AITC202006020.
3 R. Zhang, X. Zhu, H. Bai and K. Ning, Network pharmacology databases for traditional chinese medicine: review and assessment, *Front. Pharmacol.*, 2019, **10**, 123, DOI: 10.3389/fphar.2019.00123.
4 W. Zhang, Y. Huai, Z. Miao, A. Qian and Y. Wang, Systems pharmacology for investigation of the mechanisms of action of traditional chinese medicine in drug discovery, *Front. Pharmacol.*, 2019, **10**, 743, DOI: 10.3389/fphar.2019.00743.
5 D. Musumeci, G. N. Roviello and D. Montesarchio, An overview on hmgb1 inhibitors as potential therapeutic agents in hmgb1-related pathologies, *Pharmacol. Ther.*, 2014, **141**, 347–357, DOI: 10.1016/j.pharmthera.2013.11.001.
6 X. Li, Y. Yue, Y. Zhu and S. Xiong, Extracellular, but not intracellular hmgb1, facilitates self-dna induced macrophage activation via promoting dna accumulation in endosomes and contributes to the pathogenesis of lupus nephritis, *Mol. Immunol.*, 2015, **65**, 177–188, DOI: 10.1016/j.molimm.2015.01.023.
7 T. Maekawa, S. Kosuge, A. Karino, T. Okano, J. Ito, H. Munakata and K. Ohtsuki, Biochemical characterization of 60s acidic ribosomal p proteins from porcine liver and the inhibition of their immunocomplex formation with sera from systemic lupus erythematosus (sle) patients by glycyrrhizin in vitro, *Biol. Pharm. Bull.*, 2000, **23**, 27–32, DOI: 10.1248/bpb.23.27.
8 L. Zhang, P. Qing, H. Yang, Y. Wu, Y. Liu and Y. Luo, Gut microbiome and metabolites in systemic lupus erythematosus: link, mechanisms and intervention, *Front. Immunol.*, 2021, **12**, 686501, DOI: 10.3389/fimmu.2021.686501.
9 G. J. Silverman, J. Deng and D. F. Azzouz, Sex-dependent lupus blautia (ruminococcus) gnavus strain induction of zonulin-mediated intestinal permeability and autoimmunity, *Front. Immunol.*, 2022, **13**, 897971, DOI: 10.3389/fimmu.2022.897971.
10 S.-C. Choi, J. Brown, M. Gong, Y. Ge, M. Zadeh, W. Li, B. P. Croker, G. Michailidis, T. J. Garrett, M. Mohamadzadeh and L. Morel, Gut microbiota dysbiosis and altered tryptophan catabolism contribute to autoimmunity in lupus-susceptible mice, *Sci. Transl. Med.*, 2020, **12**, eaax2220, DOI: 10.1126/scitranslmed.aax2220.
11 D. F. Zegarra-Ruiz, A. El Beidaq, A. J. Iñiguez, M. Lubrano Di Ricco, S. Manfredo Vieira, W. E. Ruff, D. Mubiru, R. L. Fine, J. Sterpka, T. M. Greiling, C. Dehner and M. A. Kriegel, A diet-sensitive commensal lactobacillus strain mediates tlr7-dependent systemic autoimmunity, *Cell Host Microbe*, 2019, **25**, 113–127, DOI: 10.1016/j.chom.2018.11.009.
12 J. Rodríguez-Carrio, P. López, B. Sánchez, S. González, M. Gueimonde, A. Margolles, C. G. de Los Reyes-Gavilán and A. Suárez, Intestinal dysbiosis is associated with altered short-chain fatty acids and serum-free fatty acids in systemic lupus erythematosus, *Front. Immunol.*, 2017, **8**, 23, DOI: 10.3389/fimmu.2017.00023.
13 N. N. Nguyen, C.-Y. Lin, W.-L. Tsai, H.-Y. Huang, C.-M. Chen, Y.-T. Tung and Y.-C. Chen, Natural sweetener glycyrrhizin protects against precocious puberty by modulating the gut microbiome, *Life Sci.*, 2024, **350**, 122789, DOI: 10.1016/j.lfs.2024.122789.
14 D. S. Wishart, Y. D. Feunang, A. C. Guo, E. J. Lo, A. Marcu, J. R. Grant, T. Sajed, D. Johnson, C. Li, Z. Sayeeda, N. Assempour, I. Iynkkaran, Y. Liu, A. Maciejewski, N. Gale, A. Wilson, L. Chin, R. Cummings, D. Le, A. Pon, C. Knox and M. Wilson, DrugBank 5.0: a major update to the drugbank database for 2018, *Nucleic Acids Res.*, 2018, **46**, D1074–D1082, DOI: 10.1093/nar/gkx1037.
15 T. UniProt Consortium, UniProt: the universal protein knowledgebase, *Nucleic Acids Res.*, 2018, **46**, 2699, DOI: 10.1093/nar/gky092.
16 C. A. Lipinski, F. Lombardo, B. W. Dominy and P. J. Feeney, Experimental and computational approaches to estimate solubility and permeability in drug discovery and development settings, *Adv. Drug Delivery Rev.*, 2001, **46**, 3–26, DOI: 10.1016/s0169-409x(00)00129-0.

 This journal is © The Royal Society of Chemistry 2025

Open Access Article. Published on 09 September 2025. Downloaded on 1/11/2026 8:00:54 PM.
This article is licensed under a Creative Commons Attribution-NonCommercial 3.0 Unported Licence.

17 T. Fang, S. Liu, L. Chen, Y. Ren, D. Lu, X. Yao, T. Hong, X. Zhang, Z. Xie, K. Yang and X. Wang, Whole-genome bisulfite sequencing identified the key role of the src family tyrosine kinases and related genes in systemic lupus erythematosus, *Genes Genomics*, 2023, **45**, 1187–1196, DOI: 10.1007/s13258-023-01407-4.

18 W. Ren, G. Liu, S. Chen, J. Yin, J. Wang, B. Tan, G. Wu, F. W. Bazer, Y. Peng, T. Li, R. J. Reiter and Y. Yin, Melatonin signaling in t cells: functions and applications, *J. Pineal Res.*, 2017, **62**, e12394, DOI: 10.1111/jpi.12394.

19 C.-N. Zhao, P. Wang, Y.-M. Mao, Y.-L. Dan, Q. Wu, X.-M. Li, D.-G. Wang, C. Davis, W. Hu and H.-F. Pan, Potential role of melatonin in autoimmune diseases, *Cytokine Growth Factor Rev.*, 2019, **48**, 1–10, DOI: 10.1016/j.cytogfr.2019.07.002.

20 J. Yang, J.-M. Zhu, S. Wu, J. Li, M.-R. Wang, T.-T. Wang and Y.-W. Lu, Association study between the tp53 rs1042522 g/c polymorphism and susceptibility to systemic lupus erythematosus in a chinese han population, *Rheumatol. Int.*, 2017, **37**, 523–529, DOI: 10.1007/s00296-017-3662-0.

21 X. Qiao, Q. Wang, S. Wang, Y. Kuang, K. Li, W. Song and M. Ye, A 42-markers pharmacokinetic study reveals interactions of berberine and glycyrrhizic acid in the anti-diabetic chinese medicine formula gegen-qinlian decoction, *Front. Pharmacol.*, 2018, **9**, 622, DOI: 10.3389/fphar.2018.00622.

22 Q. Zhang, Y. Chen, Q. Wang, Y. Wang, W. Feng, L. Chai, J. Liu, D. Li, H. Chen, Y. Qiu, N. Shen, X. Shi, X. Xie and M. Li, HMGB1-induced activation of er stress contributes to pulmonary artery hypertension in vitro and in vivo, *Respir. Res.*, 2023, **24**, 149, DOI: 10.1186/s12931-023-02454-x.

23 S. Heidari, S. Mehri and H. Hosseinzadeh, The genus glycyrrhiza (fabaceae family) and its active constituents as protective agents against natural or chemical toxicities, *Phytother. Res.*, 2021, **35**, 6552–6571, DOI: 10.1002/ptr.7238.

24 M. N. Asl and H. Hosseinzadeh, Review of pharmacological effects of glycyrrhiza sp. and its bioactive compounds, *Phytother. Res.*, 2008, **22**, 709–724, DOI: 10.1002/ptr.2362.

25 A. Hevia, C. Milani, P. López, A. Cuervo, S. Arboleya, S. Duranti, F. Turroni, S. González, A. Suárez, M. Gueimonde, M. Ventura, B. Sánchez and A. Margolles, Intestinal dysbiosis associated with systemic lupus erythematosus, *mBio*, 2014, **5**, e01548–e01514, DOI: 10.1128/mBio.01548-14.

26 M. M. Li, R. R. White, L. L. Guan, L. Harthan and M. D. Hanigan, Metatranscriptomic analyses reveal ruminal ph regulates fiber degradation and fermentation by shifting the microbial community and gene expression of carbohydrate-active enzymes, *Anim. Microbiome*, 2021, **3**, 32, DOI: 10.1186/s42523-021-00092-6.

27 Y. Lan, S. Pan, B. Chen, F. Zhou, F. Yang, S. Chao, Y. Hua and H. Liu, The relationship between gut microbiota, short-chain fatty acids, and glucolipid metabolism in pregnant women with large for gestational age infant, *J. Appl. Microbiol.*, 2023, **134**, lxad240, DOI: 10.1093/jambio/lxad240.

28 S.-M. Zhang and S.-L. Huang, the commensal anaerobe veillonella dispar reprograms its lactate metabolism and short-chain fatty acid production during the stationary phase, *Microbiol. Spectrum*, 2023, **11**, e0355822, DOI: 10.1128/spectrum.03558-22.

29 C. C. Naidoo, G. R. Nyawo, I. Sulaiman, B. G. Wu, C. T. Turner, K. Bu, Z. Palmer, Y. Li, B. W. P. Reeve, S. Moodley, J. G. Jackson, J. Limberis, A. H. Diacon, P. D. van Helden, J. C. Clemente, R. M. Warren, M. Noursadeghi, L. N. Segal and G. Theron, Anaerobe-enriched gut microbiota predicts pro-inflammatory responses in pulmonary tuberculosis, *EBioMedicine*, 2021, **67**, 103374, DOI: 10.1016/j.ebiom.2021.103374.

30 K. Coello, T. H. Hansen, N. Sørensen, N. M. Ottesen, K. W. Miskowiak, O. Pedersen, L. V. Kessing and M. Vinberg, Affective disorders impact prevalence of flavonifractor and abundance of christensenellaceae in gut microbiota, *Prog. Neuropsychopharmacol. Biol. Psychiatry.*, 2021, **110**, 110300, DOI: 10.1016/j.pnpbp.2021.110300.

31 G. S. Asadi, R. Abdizadeh and T. Abdizadeh, Investigation of a set of flavonoid compounds as helicobacter pylori urease inhibitors: insights from in silico studies, *J. Biomol. Struct. Dyn.*, 2023, 1–23, DOI: 10.1080/07391102.2023.2295973.

32 D. Azzouz, A. Omarbekova, A. Heguy, D. Schwudke, N. Gisch, B. H. Rovin, R. Caricchio, J. P. Buyon, A. V. Alekseyenko and G. J. Silverman, Lupus nephritis is linked to disease-activity associated expansions and immunity to a gut commensal, *Ann. Rheum. Dis.*, 2019, **78**, 947–956, DOI: 10.1136/annrheumdis-2018-214856.

33 D. F. Azzouz, Z. Chen, P. M. Izmirly, L. A. Chen, Z. Li, C. Zhang, D. Mieles, K. Trujillo, A. Heguy, A. Pironti, G. G. Putzel, D. Schwudke, D. Fenyo, J. P. Buyon, A. V. Alekseyenko, N. Gisch and G. J. Silverman, Longitudinal gut microbiome analyses and blooms of pathogenic strains during lupus disease flares, *Ann. Rheum. Dis.*, 2023, **82**, 1315–1327, DOI: 10.1136/ard-2023-223929.

34 S. Garcia-Rodriguez, J.-L. Callejas-Rubio, N. Ortego-Centeno, E. Zumaquero, R. Ríos-Fernandez, S. Arias-Santiago, P. Navarro, J. Sancho and M. Zubiaur, Altered akt1 and mapk1 gene expression on peripheral blood mononuclear cells and correlation with t-helper-transcription factors in systemic lupus erythematosus patients, *Mediators Inflammation*, 2012, **2012**, 495934, DOI: 10.1155/2012/495934.

35 W. Hu and X. Chen, Identification of hub ferroptosis-related genes and immune infiltration in lupus nephritis using bioinformatics, *Sci. Rep.*, 2022, **12**, 18826, DOI: 10.1038/s41598-022-23730-8.

36 G. Zamolo, M. Coklo, D. Santini Dusevic, M. Kastelan, T. Batinac, E. Materljan and G. Brumini, Expression of p53 and apoptosis in discoid lupus erythematosus, *Croat. Med. J.*, 2005, **46**, 678–684.

37 D. Ghosh, G. C. Tsokos and V. C. Kyttaris, C-jun and ets2 proteins regulate expression of spleen tyrosine kinase in t cells, *J. Biol. Chem.*, 2012, **287**, 11833–11841, DOI: 10.1074/jbc.M111.333997.

Open Access Article. Published on 09 September 2025. Downloaded on 1/11/2026 8:00:54 PM.
This article is licensed under a Creative Commons Attribution-NonCommercial 3.0 Unported Licence.

38 A. Alunno, I. Padjen, A. Fanouriakis and D. T. Boumpas, Pathogenic and therapeutic relevance of jak/stat signaling in systemic lupus erythematosus: integration of distinct inflammatory pathways and the prospect of their inhibition with an oral agent, *Cells*, 2019, **8**, 898, DOI: 10.3390/cells8080898.

39 L. D. Lu, K. L. Stump, N. H. Wallace, P. Dobrzanski, C. Serdikoff, D. E. Gingrich, B. J. Dugan, T. S. Angeles, M. S. Albom, J. L. Mason, M. A. Ator, B. D. Dorsey, B. A. Ruggeri and M. M. Seavey, Depletion of autoreactive plasma cells and treatment of lupus nephritis in mice using cep-33779, a novel, orally active, selective inhibitor of jak2, *J. Immunol.*, 2011, **187**, 3840–3853, DOI: 10.4049/jimmunol.1101228.

40 S. Xiang, Y. Qu, S. Qian, R. Wang, Y. Wang, Y. Jin, J. Li and X. Ding, Association between systemic lupus erythematosus and disruption of gut microbiota: a meta-analysis, *Lupus Sci. Med.*, 2022, **9**, e000599, DOI: 10.1136/lupus-2021-000599.

41 F. Wei, H. Xu, C. Yan, C. Rong, B. Liu and H. Zhou, Changes of intestinal flora in patients with systemic lupus erythematosus in northeast china, *PLoS One*, 2019, **14**, e0213063, DOI: 10.1371/journal.pone.0213063.

42 J. R. P. Vieira, A. T. d. O. Rezende, M. R. Fernandes and N. A. da Silva, Intestinal microbiota and active systemic lupus erythematosus: a systematic review, *Adv. Rheumatol.*, 2021, **61**, 42, DOI: 10.1186/s42358-021-00201-8.

43 E. Toumi, B. Goutorbe, A. Plauzolles, M. Bonnet, S. Mezouar, M. Militello, J.-L. Mege, L. Chiche and P. Halfon, Gut microbiota in systemic lupus erythematosus patients and lupus mouse model: a cross species comparative analysis for biomarker discovery, *Front. Immunol.*, 2022, **13**, 943241, DOI: 10.3389/fimmu.2022.943241.

44 J.-W. Kim, S.-K. Kwok, J.-Y. Choe and S.-H. Park, Recent advances in our understanding of the link between the intestinal microbiota and systemic lupus erythematosus, *Int. J. Mol. Sci.*, 2019, **20**, 4871, DOI: 10.3390/ijms20194871.

45 P. López, B. de Paz, J. Rodríguez-Carrio, A. Hevia, B. Sánchez, A. Margolles and A. Suárez, Th17 responses and natural igm antibodies are related to gut microbiota composition in systemic lupus erythematosus patients, *Sci. Rep.*, 2016, **6**, 24072, DOI: 10.1038/srep24072.

46 J. J. Bunker, C. Drees, A. R. Watson, C. H. Plunkett, C. R. Nagler, O. Schneewind, A. M. Eren and A. Bendelac, B cell superantigens in the human intestinal microbiota, *Sci. Transl. Med.*, 2019, **11**, eaau9356, DOI: 10.1126/scitranslmed.aau9356.

47 H. Zhang, X. Liao, J. B. Sparks and X. M. Luo, Dynamics of gut microbiota in autoimmune lupus, *Appl. Environ. Microbiol.*, 2014, **80**, 7551–7560, DOI: 10.1128/AEM.02676-14.

48 C. R. C. van Roeyen, T. Ostendorf and J. Floege, The platelet-derived growth factor system in renal disease: an emerging role of endogenous inhibitors, *Eur. J. Cell Biol.*, 2012, **91**, 542–551, DOI: 10.1016/j.ejcb.2011.07.003.

49 T. Ostendorf, F. Eitner and J. Floege, The pdgf family in renal fibrosis, *Pediatr. Nephrol.*, 2012, **27**, 1041–1050, DOI: 10.1007/s00467-011-1892-z.

50 M.-K. Kang, S. S. Lim, J.-Y. Lee, K. M. Yeo and Y.-H. Kang, Anthocyanin-rich purple corn extract inhibit diabetes-associated glomerular angiogenesis, *PLoS One*, 2013, **8**, e79823, DOI: 10.1371/journal.pone.0079823.

51 C. Lavoz, M. Alique, R. Rodrigues-Diez, J. Pato, G. Keri, S. Mezzano, J. Egido and M. Ruiz-Ortega, Gremlin regulates renal inflammation via the vascular endothelial growth factor receptor 2 pathway, *J. Pathol.*, 2015, **236**, 407–420, DOI: 10.1002/path.4537.

52 X.-Y. Zhu, A. R. Chade, M. Rodriguez-Porcel, M. D. Bentley, E. L. Ritman, A. Lerman and L. O. Lerman, Cortical microvascular remodeling in the stenotic kidney: role of increased oxidative stress, *Arterioscler., Thromb., Vasc. Biol.*, 2004, **24**, 1854–1859, DOI: 10.1161/01.ATV.0000142443.52606.81.

53 A. L. Deluque, B. M. Oliveira, C. S. Souza, A. L. D. Maciel, H. D. C. Francescato, C. Giovanini, L. F. de Almeida, F. J. A. de Paula, R. S. Costa, J. Antunes-Rodrigues and T. M. Coimbra, Paricalcitol improves the angiopoietin/tie-2 and vegf/vegfr2 signaling pathways in adriamycin-induced nephropathy, *Nutrients*, 2022, **14**, 5316, DOI: 10.3390/nu14245316.

54 F. Liu, L. Wang, H. Qi, J. Wang, Y. Wang, W. Jiang, L. Xu, N. Liu and S. Zhuang, Nintedanib, a triple tyrosine kinase inhibitor, attenuates renal fibrosis in chronic kidney disease, *Clin. Sci.*, 2017, **131**, 2125–2143, DOI: 10.1042/CS20170134.

55 S. G. Rhee, Regulation of phosphoinositide-specific phospholipase c, *Annu. Rev. Biochem.*, 2001, **70**, 281–312, DOI: 10.1146/annurev.biochem.70.1.281.

56 N. Yang, N. J. Hong and J. L. Garvin, Dietary fructose enhances angiotensin ii-stimulated na+ transport via activation of pkc-α in renal proximal tubules, *Am. J. Physiol. Renal Physiol.*, 2020, **318**, F1513–F1519, DOI: 10.1152/ajprenal.00543.2019.

57 C. Zhang, X. He, S. R. Murphy, H. Zhang, S. Wang, Y. Ge, W. Gao, J. M. Williams, A. M. Geurts, R. J. Roman and F. Fan, Knockout of dual-specificity protein phosphatase 5 protects against hypertension-induced renal injury, *J. Pharmacol. Exp. Ther.*, 2019, **370**, 206–217, DOI: 10.1124/jpet.119.258954.

58 S. C. W. Tang, J. C. K. Leung and K. N. Lai, Diabetic tubulopathy: an emerging entity, *Contrib. Nephrol.*, 2011, **170**, 124–134, DOI: 10.1159/000325647.

59 J. C. Jha, A. Dai, J. Garzarella, A. Charlton, S. Urner, J. A. Østergaard, J. Okabe, C. E. Holterman, A. Skene, D. A. Power, E. I. Ekinci, M. T. Coughlan, H. H. H. W. Schmidt, M. E. Cooper, R. M. Touyz, C. R. Kennedy and K. Jandeleit-Dahm, Independent of renox, nox5 promotes renal inflammation and fibrosis in diabetes by activating ros-sensitive pathways, *Diabetes*, 2022, **71**, 1282–1298, DOI: 10.2337/db21-1079.

60 S. Yung, Q. Zhang, M. K. M. Chau and T. M. Chan, Distinct effects of mycophenolate mofetil and cyclophosphamide

 This journal is © The Royal Society of Chemistry 2025

Open Access Article. Published on 09 September 2025. Downloaded on 1/11/2026 8:00:54 PM.
This article is licensed under a Creative Commons Attribution-NonCommercial 3.0 Unported Licence.

on renal fibrosis in nzbwf1/j mice, *Autoimmunity*, 2015, **48**, 471–487, DOI: 10.3109/08916934.2015.1054027.

61 S. Sun, X. Ning, Y. Zhai, R. Du, Y. Lu, L. He, R. Li, W. Wu, W. Sun and H. Wang, Egr-1 mediates chronic hypoxia-induced renal interstitial fibrosis via the pkc/erk pathway, *Am. J. Nephrol.*, 2014, **39**, 436–448, DOI: 10.1159/000362249.

62 S. F. Steinberg, Structural basis of protein kinase c isoform function, *Physiol. Rev.*, 2008, **88**, 1341–1378, DOI: 10.1152/physrev.00034.2007.

63 A. C. Newton, Protein kinase c: perfectly balanced, *Crit. Rev. Biochem. Mol. Biol.*, 2018, **53**, 208–230, DOI: 10.1080/10409238.2018.1442408.

64 O. A. Ahmed-Farid, S. A. Haredy, R. M. Niazy, R. J. Linhardt and M. Warda, Dose-dependent neuroprotective effect of oriental phyto-derived glycyrrhizin on experimental neuro-terminal norepinephrine depletion in a rat brain model, *Chem.-Biol. Interact.*, 2019, **308**, 279–287, DOI: 10.1016/j.cbi.2019.05.045.

65 T. Yang, J. Zhou, L. Fang, M. Wang, M. Dilinuer and A. Ainiwaer, Protection function of 18β-glycyrrhetinic acid on rats with high-altitude pulmonary hypertension based on ^{1}H NMR metabonomics technology, *Anal. Biochem.*, 2021, **631**, 114342, DOI: 10.1016/j.ab.2021.114342.

66 Y. Mano, K. Abe, M. Takahashi, T. Higurashi, Y. Kawano, S. Miyazaki and A. Maeda-Minami, Optimal Administration of Glycyrrhizin Avoids Pharmacokinetic Interactions with High-dose Methotrexate and Exerts a Hepatoprotective Effect, *Anticancer Res.*, 2023, **43**, 1493–1501, DOI: 10.21873/anticanres.16298.

67 F. K. Alharbi, L. S. Ali, G. A. Salem, N. ElAshmouny, S. S. El-Kholy, W. M. Essawi, A. I. Helal, H. S. A. Ibrahim, N. Dahran, E. S. El-Shetry, R. H. M. Soliman, H. Emam, M. Eldesoqui, F. G. Elsaid, F. A. Al-Salmi, D. Abdelrahaman, E. Fayad, A.-R. A. Sobeih and W. A. M. Ghonimi, Glycyrrhizin alleviated cisplatin-induced testicular injury by inhibiting the oxidative, apoptotic, hormonal, and histological alterations, *Am. J. Vet. Res.*, 2025, **86**(1), DOI: 10.2460/ajvr.24.10.0288.

68 K. Holvik, S. Henjum, T. H. Stea, L. Frøyland, M. Haugen, T. Strand, M. Løvik and I. T. Lillegaard, Assessment of Dietary Intake of Potassium in Relation to Upper Guidance Level, *Eur. J. Food Res. Rev.*, 2018, DOI: 10.9734/EJNFS/2018/42534.

69 L. Castle, R. Shah, M. J. F. Fernández, C. Lambré, R. Gürtler, K. Engel, A. Christodoulidou, D. Wölfle, W. Mennes, P. Fowler, U. Gundert-Remy, P. Moldéus, A. Oskarsson, G. Aquilina, I. Waalkens-Berendsen, P. Fürst, T. Husøy and M. Younes, Opinion on the follow–up of the re–evaluation of sorbic acid (E200) and potassium sorbate (E202) as food additives, *EFSA J.*, 2019, **17**, e05625, DOI: 10.2903/j.efsa.2019.5625.